Applied Catalysis B: Environmental 258 (2019) 117979

Contents lists available at ScienceDirect

Applied Catalysis B: Environmental

journal homepage: www.elsevier.com/locate/apcatb

Incorporation of iron hydrogenase active sites into a stable photosensitizing metal-organic framework for enhanced hydrogen production

Wenjing Wang[a,d], Xiao-Wei Song[c], Zixiao Hong[b], Beibei Li[a,d], Yanan Si[a,d], Chunqing Ji[a,d], Kongzhao Su[a], Yanxi Tan[a], Zhanfeng Ju[a], Yiyin Huang[a], Chang-Neng Chen[a], Daqiang Yuan[a,*]

[a] State Key Laboratory of Structure Chemistry, Fujian Institute of Research on the Structure of Matter, Chinese Academy of Sciences, Fuzhou, 350002, Fujian, China
[b] Institute of Urban Environment, Chinese Academy of Sciences, Xiamen, 361021, Fujian, China
[c] Key Laboratory of Functional Coordination Compounds of Anhui Higher Education Institutes, Anqing Normal University, Anqing, 246011, Anhui, China
[d] University of Chinese Academy of Sciences, Beijing, 100049, China

ARTICLE INFO

Keywords:
[FeFe]-hydrogenases
Hydrogen evolution
Visible-light catalysis
Metal-organic framework

ABSTRACT

We have successfully integrated a covalently bonded hydrogen evolving catalyst (**Complex A**) into a highly stable photosensitizable **UiO-MOF** by a facile click reaction synthesis. The **UiO-MOF** was constructed from mixed functional dicarboxylate ligands, in which a $[Ru(bpy)_3]^{2+}$-derived dicarboxylate ligand (**H_2L1**) acts as a photosensitizer and an azide-modified dicarboxylate ligand (**H_2L2**) allows the catalyst **Complex A** to be firmly bound to the framework by covalent bonds. The integration of the photosensitizer and catalyst molecules together into the same **UiO-MOF** decreases the distance between them, and leads to improvement of the electron transfer efficiency between the photosensitizer and the Fe_2S_2 catalytic site. Reference experiments show that the resultant **UiO-MOF-Fe_2S_2** exhibits exponentially enhanced photocatalytic activity and stability in a visible-light driven hydrogen process. The excellent performance of the **UiO-MOF-Fe_2S_2** indicates that incorporation of the Fe_2S_2 catalytic center into **UiO-MOF** is a promising strategy with which to stabilize Fe_2S_2 catalyst in water and improve the photocatalytic efficiency of hydrogen evolution.

1. Introduction

[FeFe]-hydrogenase, an excellent natural biological enzyme catalyst, is highly efficient in reducing protons to hydrogen and demonstrates remarkable turnover frequencies, on the order of 6000–9000 molecules H_2 per active site per second [1]. Since the first artificial photocatalytic system used for hydrogen production was constructed by Sun and Åkermark in 2003, many efforts have been undertaken to design and optimize the structure and functionality of [FeFe]-hydrogenase in pursuit of high activity in the hydrogen production process [2–8]. To date however, there are still no artificial [FeFe]-hydrogenase mimics that can reproduce the high reactivity of natural [FeFe]-hydrogenase. Recently, Wu et al. have shown that improving the electron transfer between a photosensitizer and [FeFe]-hydrogenase catalyst in a local microenvironment could provide a promising approach to increasing hydrogen production [9,10], and, in addition to its extensively investigated structure, the external matrix of [FeFe]-hydrogenase has also attracted our attention.

Emerging as an intriguing class of porous crystalline materials, metal-organic frameworks (MOFs), also known as porous coordination polymers, can be easily functionalized at the molecular level. [11–14] Over the past two decades, MOFs have received significant attention owing to their various applications including gas storage [15–17], separation [18–20], chemical sensing [21–23], drug delivery [24,25], and catalysis [26–32]. Functional molecular building blocks can be incorporated into MOFs in the form of bridging ligands [33,34] or secondary building units (SBU) [35]. In addition, functional entities can also be attached to the walls of MOFs by post-synthetic modifications [36–39] or into the channels and cavities as counterions [40] or trapped nanoparticles [41]. Incorporation of catalytic sites into MOFs to create heterogeneous catalysts has played an important role in a wide range of chemical reactions [42–44]. Compared with homogeneous catalysts, heterogeneous catalysts possess some special advantages, such as enhanced stability, easy separation and efficient recycling [30,31]. In the photocatalytic hydrogen evolution process, integrating catalytic active sites and photosensitizers into MOFs as a heterogeneous catalyst for hydrogen production has shown a greater improved activity and stability than homogeneous catalysts. For example, Ir or Ru polypyridine complexes as photosensitizers have been incorporated in MOFs to drive photochemical hydrogen production catalyzed by a Pt complex

* Corresponding author.
E-mail address: ydq@fjirsm.ac.cn (D. Yuan).

https://doi.org/10.1016/j.apcatb.2019.117979
Received 7 May 2019; Received in revised form 25 June 2019; Accepted 18 July 2019
Available online 19 July 2019
0926-3373/

[33], Pt nanoparticles [45] or polyoxometalates [43,46]. In order to reduce the use of noble metal catalysts in the hydrogen evolution process, Cohen and Ott incorporated Fe_2S_2, a hydrogenase biomimetic into MOFs by post-synthetic exchange, and demonstrated improved photocatalytic activity and stability for hydrogen production with $[Ru(bpy)_3]^{2+}$ as a photosensitizer [47]. Subsequently, Feng introduced an $[Fe_2S_2]$ complex into a zirconium-porphyrin MOF by direct coordination, to form a new hydrogen evolution material which acts both as a photosensitizer and catalyst [48]. Recently, Ott et al. have made an $[Fe_2S_2]$ catalyst attached covalently through an amide bond to an amino-functionalized MIL-101(Cr) [49]. Different proportions of the catalyst loading in MIL-101-NH-[FeFe] exhibit better catalytic activity performance compared with the homogeneous reference system $[Fe_2(dcbdt)(CO)_6]$. Although some advances have been made in combination of $[Fe_2S_2]$ catalyst and MOFs, it is still a challenging task to obtain a new hydrogen evolving catalyst with high stability and activity. However, introduction of $[Fe_2S_2]$ catalyst into photosensitizing MOF by covalent bonds has been rarely reported to date. In this paper, we report the incorporation of an $[Fe_2S_2]$ catalytic site into an $[Ru(bpy)_3]^{2+}$-derived photosensitizing UiO-type MOF by a facile click reaction to generate a new hydrogen evolution catalyst **UiO-MOF-Fe_2S_2** (Scheme 1). The rationale for this is mainly based on the following considerations: (a) Zr-based UiO-MOFs exhibit exceptionally high structural stability under aqueous and weakly acidic conditions; (b) the $[Fe_2S_2]$ catalytic active site linked by a covalent bond is stronger than a link based on a coordination bond and guarantees that the catalytic site is bound tightly to the framework; (c) having the integrating photosensitizer and catalytic site in the same framework could improve the electron transfer process and thus enhance the efficiency of hydrogen evolution; (d) the protection of the framework around the Fe_2S_2 sites could improve the stability of the $[Fe_2S_2]$ catalyst; (e) the amount of $[Fe_2S_2]$ catalytic active site is easier to control compared with ligand exchange or weakly coordination strategy. In the presence of ascorbic acid (100 mM) as a proton source and a sacrificial electron donor, the **UiO-MOF-Fe_2S_2** shows an enhanced hydrogen evolution efficiency and improved stability of catalyst in water compared to analogous reference systems.

2. Experimental

2.1. Catalyst preparation

2.1.1. Synthesis of MOF-N_3

H_2L2 (2″-(azidomethyl)-[1,1′:4′,1″:4″,1‴-quaterphenyl]-4,4‴-dicarboxylic acid, 5.0 mg, 11.1 μmol), $ZrCl_4$ (5.0 mg, 21.5 μmol), and trifluoroacetic acid (30 μL, 0.4 mmol) were dissolved in 2.0 mL DMF then sealed in a 5.0 mL vial, and placed in an oven at 100 °C. The vial was heated at 100 °C for 48 h. After cooling to room temperature, the crystalline solid **MOF-N_3** was isolated by decanting the supernatant solution and then was washed with DMF, MeOH, and H_2O repeatedly. Yield: 30%.

2.1.2. Synthesis of UiO-MOF

H_2L1 (8.8 mg, 11 μmol), **H_2L2** (4.5 mg, 11 μmol), $ZrCl_4$ (5.0 mg, 22 μmol), and trifluoroacetic acid (30 μL, 0.4 mmol) were dissolved in 2.0 mL DMF, sealed in a 5.0 mL vial, and placed in a 100 °C oven. The vial was heated at 100 °C for 48 h. After cooling to room temperature, the crystalline solid **UiO-MOF** was isolated by decanting the supernatant solution and then was washed with DMF, MeOH, and H_2O repeatedly. Yield: 35%.

2.1.3. Synthesis of UiO-MOF-Fe_2S_2

A flask was charged with a mixture of **UiO-MOF** (0.071 g, 10 μmol), **Complex A** (0.01 g, 20 μmol), CuI (0.002 g, 10.5 μmol) and DMF (3.0 mL). The mixture was heated at 70 °C with magnetic stirring for 24 h under Ar protection. After cooling to room temperature, the crystalline solid **UiO-MOF-Fe_2S_2** was isolated by centrifugation and washed thoroughly with DMF and Me_2CO.

2.2. Photocatalytic reaction

A reaction vessel was charged with 100 mL acetate buffer solution (1.0 M, pH = 5.0) and ascorbic acid (1.76 g, 100 mM) and ground catalyst **UiO-MOF-Fe_2S_2** (0.015 g, 2 μmol) was added. The temperature of the mixture was controlled at 10 °C and, after the reaction system was evacuated, the reaction vessel was irradiated by a solid-state white light source with a long-pass filter (λ > 420 nm). The H_2 produced in the reaction was monitored by gas chromatography.

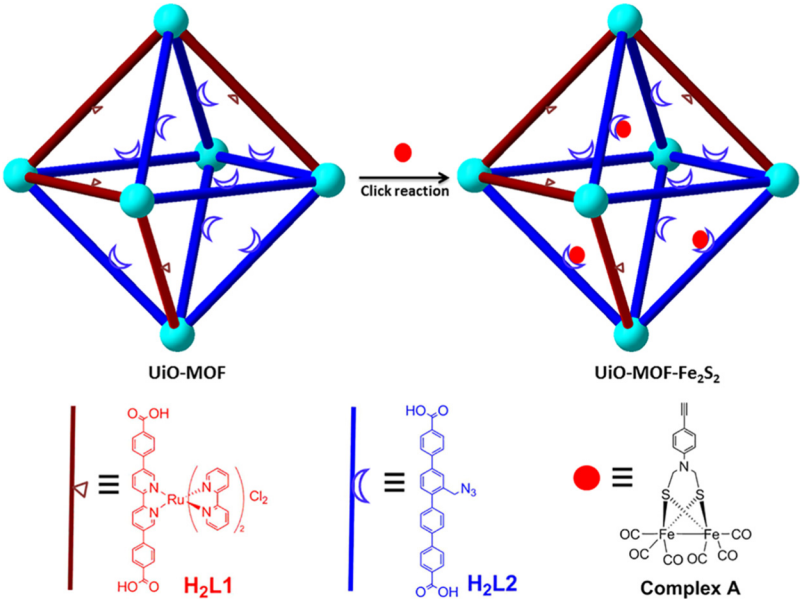

Scheme 1. Modification of **UiO-MOF** *via* a click reaction was used to form new catalysts **UiO-MOF-Fe_2S_2** incorporating $[Fe_2S_2]$ catalytic sites.

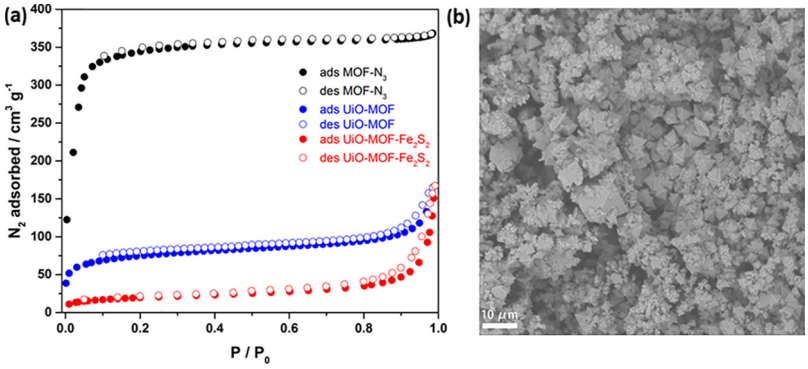

Fig. 1. (a) N_2 adsorption properties of **MOF-N$_3$**, **UiO-MOF** and **UiO-MOF-Fe$_2$S$_2$**, respectively. (b) SEM images of **UiO-MOF-Fe$_2$S$_2$**. Scale bar is 10 μm.

3. Results and discussion

3.1. Synthesis and structure

The $[Ru(bpy)_3]^{2+}$-derived dicarboxylate ligand (**H$_2$L1**) was synthesized according to the previous method (Scheme S1) [46]. We chose ligand **H$_2$L1** here because it can form a highly stable UiO type MOF, with a triangular open channel and an edge length of 1.6 nm. To introduce a catalytic center (**Complex A**) into MOFs through a click reaction, we designed and synthesized dicarboxylate ligand with a modified azide group (**H$_2$L2**) (Scheme S2 and S3). The reaction of ligand **H$_2$L2** with $ZrCl_4$ afforded a non-interpenetrated **MOF-N$_3$** whose powder X-ray diffraction (PXRD) results matched well with data from simulated TPHN-MOF (Fig. S1 in SI) [50]. The permanent porosity of **MOF-N$_3$** was proved by nitrogen adsorption at 77 K. The Brunauer-Emmett-Teller (BET) surface area of **MOF-N$_3$**, calculated from N_2 adsorption data is 1280 $m^2 g^{-1}$ (Fig. 1a). The ligand length of **H$_2$L2** matches well with that of **H$_2$L1** and facilitates efficient doping of the **H$_2$L2** ligand into the UiO framework. The sizes of open channel and cavities of MOFs make it possible for **Complex A**, with an overall diameter of ~8 Å to penetrate the MOF and reach the reaction sites.

Subsequently, equimolar amounts of ligand **H$_2$L1** and **H$_2$L2** react with CF_3COOH and $ZrCl_4$ in DMF at 100 °C for 48 h to give the highly crystalline **UiO-MOF**. Scanning electron microscopy (SEM) analysis showed that the **UiO-MOF** adopts an octahedral-shaped morphology with a particle size ranging from 0.5 to 10 μm (Fig. 1b). Powder X-ray diffraction results are shown in Fig. 2a. The peaks can be well matched with those from a simulated structure, and confirm the formation of a non-interpenetrated structure. Compared with **MOF-N$_3$**, the BET surface areas of **UiO-MOF** were drastically lower, 260 *vs.* 1280 $m^2 g^{-1}$ (Fig. 1a). This significant change is mainly the result of the successful introduction of the **H$_2$L1** ligand. The ratio of heavy elements in **UiO-MOF** was determined to be 4.36:1 for Zr:Ru, determined by inductively coupled plasma spectrometry (ICP) and supported an overall formula of $Zr_6(\mu_3\text{-}O)_4(\mu_3-OH)_4(L1)_{1.4}(L2)_{4.6}$ for **UiO-MOF** which indicates 76% incorporation of the ligand **H$_2$L2** into the **UiO-MOF**. Compared with the equimolar amounts of ligand **H$_2$L1** and **H$_2$L2** in the starting materials, the significant difference of the ratio of the ligands obtained in **UiO-MOF** can be attributed to the steric bulk of the ligand **H$_2$L1**. The ligand **H$_2$L2**, with its low steric demand is favored during **UiO-MOF** growth. In addition, the FTIR spectrum of **UiO-MOF** clearly exhibited a peak characteristic of the azide absorption band at 2100 cm^{-1}, indicating that ligand **H$_2$L2** had also been successfully incorporated into **UiO-MOF** (Fig. 2b). **UiO-MOF** with azide group loadings was allowed to react with the catalytic center (**Complex A**) in the presence of a CuI catalyst at 70 °C in DMF. After the click reaction, the products were collected by centrifugation and thoroughly washed with DMF and Me_2CO several times. The resulting dried compound produced in this manner was named **UiO-MOF-Fe$_2$S$_2$**. The Inductively Coupled Plasma (ICP) results clearly showed that very few Cu species (1.2 wt %) from the CuI catalyst remained in the product, which is consistent with earlier work. [51] Scanning Electron Microscopy (SEM), showed that the morphology of the nanoparticles was well maintained after the click reaction except for a little agglomeration (Fig. S2). In addition, PXRD studies confirmed the retention of the crystalline framework of the resultant **UiO-MOF-Fe$_2$S$_2$** after the click reaction (Fig. 2a), and meanwhile, the BET surface area of **UiO-MOF-Fe$_2$S$_2$** was further reduced to 70 $m^2 g^{-1}$ (Fig. 1a). The characteristic IR band for the azide group was sharply weakened and three new CO stretching vibration bands appeared at 1998, 2032, and 2071 cm^{-1}, suggesting the click reaction had occurred and the $[Fe_2S_2]$ catalytic center in **UiO-MOF-Fe$_2$S$_2$** remained intact. The acetylene group stretching vibration bands of **Complex A**, located at 3280 and 1962 cm^{-1} were absent in **UiO-MOF-Fe$_2$S$_2$**, which also indicated that the catalyst **Complex A** was connected by covalent chemical bonds, rather than simple being physically adsorbed on the **UiO-MOF** surface or in its pores (Fig. 2b). Finally, judging by the ICP data analysis, approximately 7.3 wt% of the **Complex A** had been successfully introduced into the **UiO-MOF**.

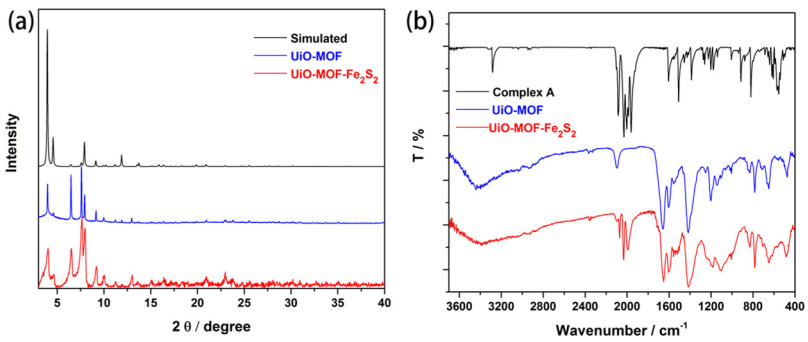

Fig. 2. (a) PXRD of **UiO-MOF**, **UiO-MOF-Fe$_2$S$_2$** and simulated data. (b) FTIR of **Complex A UiO-MOF**, **UiO-MOF-Fe$_2$S$_2$**.

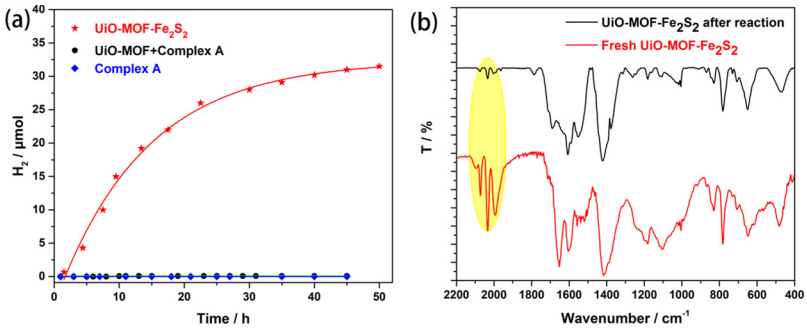

Fig. 3. (a) Photocatalytic H_2 evolution in the presence of **UiO-MOF-Fe$_2$S$_2$** (15 mg, ~2.0 μmmol catalyst), **UiO-MOF** + **Complex A** (14 mg + 1 mg, ~2.0 μmmol catalyst) and **Complex A** only (1 mg, ~2.0 μmmol). Photocatalytic conditions: Visible light (> 420 nm), pH = 5 (1.0 M acetate buffer solution), 100 mM ascorbic acid. (b) FTIR of fresh **UiO-MOF-Fe$_2$S$_2$** and after the photocatalytic sample. The highlighted area represents the CO vibration region of Fe_2S_2 catalytic sites.

3.2. Photocatalytical property

Having observed that a click reaction could be used to incorporate catalytic sites into the robust **UiO-MOF**, we subsequently investigated the viability of **UiO-MOF-Fe$_2$S$_2$** as a catalyst in photochemical hydrogen generation. The visible light-driven catalytic activities of **UiO-MOF-Fe$_2$S$_2$** were studied in a 1.0 M acetate buffer solution (pH = 5.0) in the presence of ascorbic acid (100 mM) as a sacrificial electron donor. The reaction vessel was irradiated by a solid-state white light source with a long-pass filter (λ > 420 nm). Under these reaction conditions, H_2 production was observed and the amount of H_2 produced was quantified by gas chromatography analysis. As shown in Fig. 3a, the dependence of H_2 evolution on irradiation time showed that the amount of H_2 increased in the first 20 h and then continued irradiation caused a slow improvement in the amount of H_2 production. After illuminating for 50 h, a total of 32 μmol H_2 was produced. For comparison, control experiments were also carried out and indicated that there is no obvious H_2 production in the absence of the photosensitizer center, $[Ru(bpy)_3]^{2+}$. This result indicates that the photosensitizer is necessary for a photochemical system to drive hydrogen evolution. Compared to **UiO-MOF-Fe$_2$S$_2$**, the isolated **UiO-MOF** and catalyst **Complex A** also show traces of H_2 production (Fig. 3a). Clearly, the catalyst **UiO-MOF-Fe$_2$S$_2$** exhibits high activity compared to isolated **UiO-MOF** and **Complex A**. The result also reveals that the distance between photosensitizer and catalyst is very important for H_2 production. Even if the photosensitizer and the catalyst are present in the same catalytic system, electron transfer between them is not favorable as long as the the distance between photosensitizer and catalyst is not close enough. The large difference between the catalytic activity of **UiO-MOF-Fe$_2$S$_2$** and that of isolated **UiO-MOF** and **Complex A** under the same condition indicates that the covalent bond connection between **Complex A** and **UiO-MOF** plays a vital role in the photocatalytic H_2 evolution process. The integration of photosensitizer and catalyst together into MOFs could enhance the efficiency of electron transfer. In order to understand the cause of catalyst deactivation, a sample remaining after the reaction was collected and analyzed by FTIR spectroscopy. As shown in Fig. 3b, the characteristic CO stretching vibration bands of **UiO-MOF-Fe$_2$S$_2$** became very weak and consequently, the main reason for the deactivation of the catalyst was ascribed to the decomposition of the Fe_2S_2 center. However, the catalyst **Complex A** can only survive 3 h in a homogeneous system under the same conditions, evidenced by the absence of FTIR signals in the typical CO region after the reaction (Fig. S3). Introduction of the catalyst **Complex A** into **UiO-MOF** therefore not only enhances the catalytic activity but also greatly improves the stability of the catalyst. The protection of the framework around the Fe_2S_2 sites and the shortening of the distance between the photosensitizer and the active sites of the catalyst can explain the good performance of **UiO-MOF-Fe$_2$S$_2$** [10]. Therefore, the integration of photosensitizer and catalyst together into MOFs could achieve their synergistic effects and provid a more stable catalyst and an efficient catalytic system for hydrogen evolution.

3.3. Photocatalytical mechanism

To explore the charge transfer pathways, we investigated the luminescence and lifetime of **Et$_2$L1** before and after adding **Complex A** or ascorbic acid. No decrease in the fluorescence intensity and lifetime was observed upon addition of **Complex A** (Figs. S4, S5). In contrast, the luminescence of **Et$_2$L1** was efficiently quenched by 100 mM ascorbic acid in H_2O; meanwhile, the lifetime of **Et$_2$L1** was also decreased to 591 ns from the 340 ns (Fig. 4a, b). These results indicate that the excited state of the polypyridyl ruthenium moiety $[Ru]^{2+}$ of the catalyst **UiO-MOF-Fe$_2$S$_2$** should be reductively quenched by ascorbic acid rather than oxidatively quenched by Fe_2S_2 sites. Cyclic voltammetry studies showed that **Et$_2$L1** displays four reversible reduction events at −1.58, −1.85, −1.98 and −2.23 V, which could be assigned to the bipyridine ligand-based events (Fig. S6). The onset oxidation potential of ascorbic acid is 0.28 V (*vs.* Fc^+/Fc) (Fig. S7). In addition, the energy of the triplet excited state of the photosensitizer was determined from the emission spectrum of **Et$_2$L1** to be 1.91 eV. According to the Rehm-Weller equation, the free energy change (ΔG) of the electron transfer process from the ascorbic acid to the excited photosensitizer center was estimated to be −0.05 eV, which suggests that it is thermodynamically feasible for the reductive quenching process.

Based on hydrogen production experiment and the above spectroscopic study, we can speculate on a possible mechanism of the catalytic

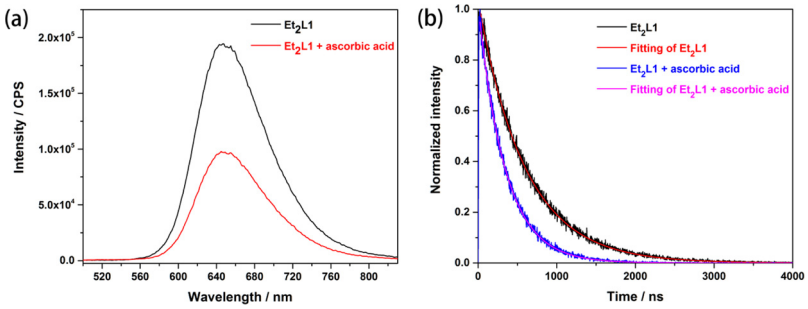

Fig. 4. (a) The fluorescent emission spectra of **Et$_2$L1** and **Et$_2$L1** + **ascorbic acid**. (b) Normalized luminescence decay traces of **Et$_2$L1** and **Et$_2$L1** + **ascorbic acid** measured at the 650 nm emission wavelength in H_2O with 470 nm excitation.

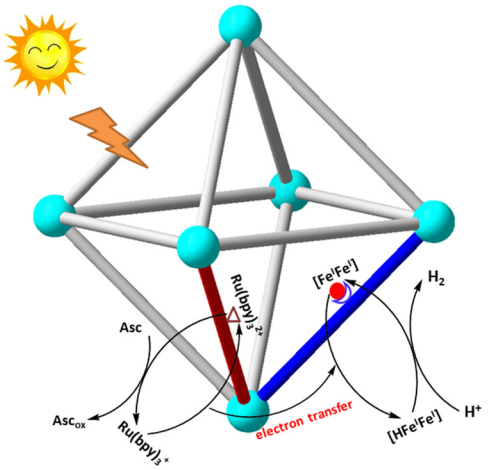

Scheme 2. Proposed photocatalytic reaction scheme for the reduction of protons.

system (Scheme 2). Upon irradiation with visible light, the polypyridyl ruthenium moiety is excited and then generated a reduced species $[Ru]^+$ by electron transfer from ascorbic acid (E = −1.58 V *vs. Fc*$^+$*/Fc* for Ru^{2+}/Ru^+), which is then capable of reducing the **Fe_2S_2** to an Fe^0Fe^I species (E = −1.55 V *vs. Fc*$^+$*/Fc*) (Fig. S8). However, considering the reduction capability of reduced species $[Ru]^+$ and the second reduction potentials of **Complex A** (E = −2.11 V *vs.* Fc^+/Fc), further reduction of Fe^0Fe^I to Fe^0Fe^0 by $[Ru]^+$ is thermodynamically unfavorable. It therefore seems that the intermediate is protonated and then accepted another electron from the polypyridyl ruthenium moiety to form $[HFe^IFe^I]$, which finally react with proton to generate H_2, accompanied by the regeneration of **Complex A** [52]. Meanwhile, the polypyridyl ruthenium moiety can be regenerated by accepting an electron from the sacrificial agent (ascorbic acid).

4. Conclusions

In summary, based on the click reaction, we have successfully incorporated a covalently bonded catalytic site (**Complex A**) into **UiO-MOF**, to form a new hydrogen evolving catalyst **UiO-MOF-Fe_2S_2**. The selection of mixed dicarboxylate ligands to construct the **UiO-MOF** was based largely on the following considerations. The $[Ru(bpy)_3]^{2+}$-derived dicarboxylate ligand (**H_2L1**) acts as a photosensitizer and an azide-modified dicarboxylate ligand (**H_2L2**) allows the catalyst **Complex A** to be firmly bound to the framework by covalent bonds. After the catalytic active site (Fe_2S_2) has been introduced into **UiO-MOF**, its catalytic stability is greatly improved by the protection from the framework. After 50 h of photocatalytic reaction, a total of 32 μmol H_2 can be produced. Compared with reference experiments, the high hydrogen production of **UiO-MOF-Fe_2S_2** can be attributed to the efficient electron transfer between the photosensitizer and the Fe_2S_2 catalytic site. The good performance of **UiO-MOF-Fe_2S_2** indicates that incorporation of the Fe_2S_2 catalytic center into **UiO-MOF** is a promising strategy with which to stabilize the Fe_2S_2 catalyst and improve the photocatalytic efficiency of hydrogen evolution in water.

Declaration of Competing Interest

The authors declare that they have no known competing financial interests or personal relationships that could have appeared to influence the work reported in this paper.

Acknowledgements

This work was supported by the Strategic Priority Research Program of the Chinese Academy of Sciences (XDB20000000), the Key Research Program of Frontier Sciences, Chinese Academy of Sciences (QYZDB-SSW-SLH019), and the National Natural Science Foundation of China (21707143, 51603206 and 21771177).

Appendix A. Supplementary data

Supplementary material related to this article can be found, in the online version, at doi:https://doi.org/10.1016/j.apcatb.2019.117979.

References

[1] M. Frey, Chembiochem 3 (2002) 153–160.
[2] S. Ott, M. Kritikos, B. Akermark, L. Sun, Angew. Chem. Int. Ed. 42 (2003) 3285–3288.
[3] L.C. Song, M.Y. Tang, F.H. Su, Q.M. Hu, Angew. Chem. Int. Ed. 45 (2006) 1130–1133.
[4] W. Gao, J. Sun, T. Akermark, M. Li, L. Eriksson, L. Sun, B. Akermark, Chem. Eur. J. 16 (2010) 2537–2546.
[5] D. Streich, Y. Astuti, M. Orlandi, L. Schwartz, R. Lomoth, L. Hammarstrom, S. Ott, Chem. Eur. J. 16 (2010) 60–63.
[6] X. Li, M. Wang, D. Zheng, K. Han, J. Dong, L. Sun, Energy Environ. Sci. 5 (2012) 8220–8224.
[7] C.-B. Li, Z.-J. Li, S. Yu, G.-X. Wang, F. Wang, Q.-Y. Meng, B. Chen, K. Feng, C.-H. Tung, L.-Z. Wu, Energy Environ. Sci. 6 (2013) 2597–2602.
[8] Y. Li, T.B. Rauchfuss, Chem. Rev. 116 (2016) 7043–7077.
[9] J.X. Jian, Q. Liu, Z.J. Li, F. Wang, X.B. Li, C.B. Li, B. Liu, Q.Y. Meng, B. Chen, K. Feng, C.H. Tung, L.Z. Wu, Nat. Commun. 4 (2013) 2695.
[10] F. Wang, W.J. Liang, J.X. Jian, C.B. Li, B. Chen, C.H. Tung, L.Z. Wu, Angew. Chem. Int. Ed. 52 (2013) 8134–8138.
[11] K.K. Tanabe, S.M. Cohen, Chem. Soc. Rev. 40 (2011) 498–519.
[12] S.M. Cohen, Chem. Rev. 112 (2012) 970–1000.
[13] Y. He, B. Li, M. O'Keeffe, B. Chen, Chem. Soc. Rev. 43 (2014) 5618–5656.
[14] S. Kitagawa, R. Kitaura, S. Noro, Angew. Chem. Int. Ed. 43 (2004) 2334–2375.
[15] M.P. Suh, H.J. Park, T.K. Prasad, D.W. Lim, Chem. Rev. 112 (2012) 782–835.
[16] K. Sumida, D.L. Rogow, J.A. Mason, T.M. McDonald, E.D. Bloch, Z.R. Herm, T.H. Bae, J.R. Long, Chem. Rev. 112 (2012) 724–781.
[17] D. Zhao, D.Q. Yuan, H.C. Zhou, Energy Environ. Sci. 1 (2008) 222–235.
[18] J.R. Li, J. Sculley, H.C. Zhou, Chem. Rev. 112 (2012) 869–932.
[19] H. Wu, Q. Gong, D.H. Olson, J. Li, Chem. Rev. 112 (2012) 836–868.
[20] J.R. Li, R.J. Kuppler, H.C. Zhou, Chem. Soc. Rev. 38 (2009) 1477–1504.
[21] L.E. Kreno, K. Leong, O.K. Farha, M. Allendorf, R.P. Van Duyne, J.T. Hupp, Chem. Rev. 112 (2012) 1105–1125.
[22] M.D. Allendorf, C.A. Bauer, R.K. Bhakta, R.J. Houk, Chem. Soc. Rev. 38 (2009) 1330–1352.
[23] J. Rocha, L.D. Carlos, F.A. Paz, D. Ananias, Chem. Soc. Rev. 40 (2011) 926–940.
[24] A.C. McKinlay, R.E. Morris, P. Horcajada, G. Ferey, R. Gref, P. Couvreur, C. Serre, Angew. Chem. Int. Ed. 49 (2010) 6260–6266.
[25] P. Horcajada, R. Gref, T. Baati, P.K. Allan, G. Maurin, P. Couvreur, G. Ferey, R.E. Morris, C. Serre, Chem. Rev. 112 (2012) 1232–1268.
[26] J. Jiang, O.M. Yaghi, Chem. Rev. 115 (2015) 6966–6997.
[27] M. Yoon, R. Srirambalaji, K. Kim, Chem. Rev. 112 (2012) 1196–1231.
[28] A.H. Chughtai, N. Ahmad, H.A. Younus, A. Laypkov, F. Verpoort, Chem. Soc. Rev. 44 (2015) 6804–6849.
[29] A. Dhakshinamoorthy, H. Garcia, Chem. Soc. Rev. 41 (2012) 5262–5284.
[30] J. Lee, O.K. Farha, J. Roberts, K.A. Scheidt, S.T. Nguyen, J.T. Hupp, Chem. Soc. Rev. 38 (2009) 1450–1459.
[31] L. Ma, C. Abney, W. Lin, Chem. Soc. Rev. 38 (2009) 1248–1256.
[32] T. Zhang, W. Lin, Chem. Soc. Rev. 43 (2014) 5982–5993.
[33] D. Kim, D.R. Whang, S.Y. Park, J. Am. Chem. Soc. 138 (2016) 8698–8701.
[34] S. Pullen, G.H. Clever, Acc. Chem. Res. 51 (2018) 3052–3064.
[35] X.L. Wang, L.Z. Dong, M. Qiao, Y.J. Tang, J. Liu, Y. Li, S.L. Li, J.X. Su, Y.Q. Lan, Angew. Chem. Int. Ed. 57 (2018) 9660–9664.
[36] L. Garzon-Tovar, S. Rodriguez-Hermida, I. Imaz, D. Maspoch, J. Am. Chem. Soc. 139 (2017) 897–903.
[37] Y. Goto, H. Sato, S. Shinkai, K. Sada, J. Am. Chem. Soc. 130 (2008) 14354–14355.
[38] Y. Zhang, B. Gui, R. Chen, G. Hu, Y. Meng, D. Yuan, M. Zeller, C. Wang, Inorg. Chem. 57 (2018) 2288–2295.
[39] U. Fluch, B.D. McCarthy, S. Ott, Dalton Trans. 48 (2019) 45–49.
[40] J. Yu, Y. Cui, H. Xu, Y. Yang, Z. Wang, B. Chen, G. Qian, Nat. Commun. 4 (2013) 2719.
[41] F. Schröder, D. Esken, M. Cokoja, M.W.E. van den Berg, O.I. Lebedev, G.V. Tendeloo, B. Walaszek, G. Buntkowsky, H.-H. Limbach, B. Chaudret, R.A. Fischer, J. Am. Chem. Soc. 130 (2008) 6119–6130.
[42] B. An, J. Zhang, K. Cheng, P. Ji, C. Wang, W. Lin, J. Am. Chem. Soc. 139 (2017) 3834–3840.
[43] X.J. Kong, Z. Lin, Z.M. Zhang, T. Zhang, W. Lin, Angew. Chem. Int. Ed. 55 (2016) 6411–6416.
[44] Q.L. Zhu, J. Li, Q. Xu, J. Am. Chem. Soc. 135 (2013) 10210–10213.
[45] C. Wang, K.E. deKrafft, W. Lin, J. Am. Chem. Soc. 134 (2012) 7211–7214.
[46] Z.M. Zhang, T. Zhang, C. Wang, Z.K. Lin, L.S. Long, W.B. Lin, J. Am. Chem. Soc. 137 (2015) 3197–3200.

[47] S. Pullen, H. Fei, A. Orthaber, S.M. Cohen, S. Ott, J. Am. Chem. Soc. 135 (2013) 16997–17003.
[48] K. Sasan, Q. Lin, C. Mao, P. Feng, Chem. Commun. (Camb.) 50 (2014) 10390–10393.
[49] S. Roy, V. Pascanu, S. Pullen, G. Gonzalez Miera, B. Martin-Matute, S. Ott, Chem. Commun. (Camb.) 53 (2017) 3257–3260.
[50] K. Manna, T. Zhang, F.X. Greene, W. Lin, J. Am. Chem. Soc. 137 (2015) 2665–2673.
[51] H.L. Jiang, D.W. Feng, T.F. Liu, J.R. Li, H.C. Zhou, J. Am. Chem. Soc. 134 (2012) 14690–14693.
[52] Y. Na, M. Wang, J. Pan, P. Zhang, B. Akermark, L. Sun, Inorg. Chem. 47 (2008) 2805–2810.